

ISSN 0007-1226 (print) / ISSN 1744-5019 (online)
http://www.biomedical-engineering-online.com

Annals of

Biomedical Engineering



The Journal of the Biomedical Engineering Society

with cooperation from the U.S. National Committee on Biomechanics

 **BMES**

Volume 35 Number 1 February 2013

Design and Fabrication of an Injection Tool for Neuromuscular Microstimulators

HILTON M. KAPLAN^{1,2} and GERALD E. LOEB¹

¹Alfred Mann Institute for Biomedical Engineering, University of Southern California, 1042 Downey Way, DRB-101, Los Angeles, CA 90089, USA; and ²PO Box 2337, Beverly Hills, CA 90213, USA

(Received 18 January 2008; accepted 6 June 2009; published online 24 June 2009)

Abstract—The injection of small implants into precisely localized sites within the body is a difficult task usually undertaken by surgeons or interventional radiologists. We have designed, produced and tested a simple tool for implanting BIONTM wireless microstimulators as an outpatient office procedure. The ability of BIONs to elicit a desired muscle contraction depends on their placement near the motor fibers that innervate the muscle fibers, providing both the requirement and a means for achieving accurate placement. The implant is preloaded into the tip of the cannula of a two-piece insertion tool made from non-conductive polymers. Trial stimulation pulses are generated by the implant as the tool is manipulated into the desired position. The implant is released by withdrawing the cannula over the implant, preserving both the relative location of the implant's electrodes with respect to the target and determining its desired axial orientation, which is important for implants containing motion sensors. The BION Insertion Tool has been used for over 30 BION implants in human subjects to date.

Keywords—BION, Stimulation, Implantation, Hypodermic needle, Finite element modeling, EMG, M-wave, Accelerometer.

ABBREVIATIONS

AMI-USC	Alfred Mann Institute at the University of Southern California
BION TM	BIONic Neuron (an injectable, wireless microstimulator)
BIT	BION Insertion Tool
FEA	Finite Element Analysis

INTRODUCTION

The BIONTM microstimulator has a cylindrical shape and miniature size (2.1 mm diameter × 16.0 mm long) to facilitate nonsurgical placement of one or more implants via percutaneous injection rather than open surgical procedures. The implant receives power and digital command signals by inductive coupling to an external transmission coil, and it generates precisely controllable electrical pulses to stimulate nearby sensory or motor nerve fibers.^{10,11} The selectivity and efficacy of stimulation depends largely on the placement of its output electrode with respect to nearby nerve fibers. Multiple BION implants have been used to produce coordinated contractions of individual muscles to prevent disuse atrophy,⁷ and to restore functional limb movements in patients with upper motor neuron lesions (e.g., stroke and spinal cord injury).⁶ We anticipate that such functional electrical stimulation will benefit eventually from closed-loop feedback from sensors incorporated into these implants,¹⁵ including multi-axial accelerometers whose axial orientation is important for their function.^{18,19}

In order to inject these devices in a simple yet highly accurate manner, we have designed, built and tested the BION Insertion Tool (BIT) described herein, which is now in clinical use (Figs. 1 and 2). A simple two-piece needle-like insertion tool houses the microstimulator, and enables stimulation pulses from the microstimulator to be delivered through its tip while the BIT is directed toward the target. The basic design is suited to implanting any cargo of similar form-factor (e.g., drug implants, chemotherapeutic agents, transplanted tissues and cell cultures, radiotherapeutic beads, etc.).

Context and History

The design detailed here evolved through several iterations based on systematic review of manufacturing and clinical experience. The resultant BIT has been

Address correspondence to Hilton M. Kaplan, PO Box 2337, Beverly Hills, CA 90213, USA. Electronic mail: hkaplan@alumni.usc.edu

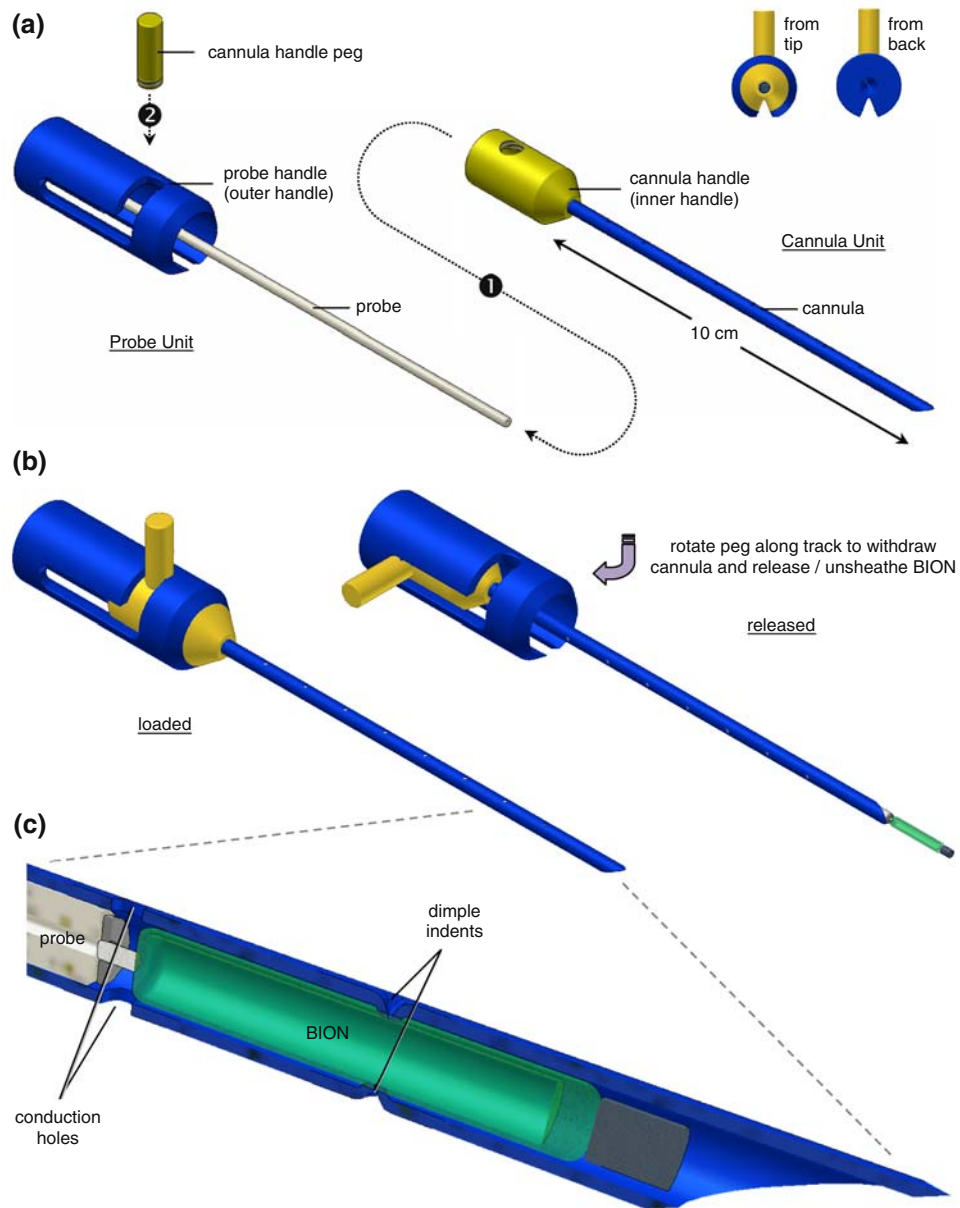


FIGURE 1. (a) The BIT comprises two units: the Cannula Unit is slid over the probe, so that its handle comes to lie within the Probe Unit's handle. The peg screws into the cannula handle through the open track in the probe handle, where it is held by locking resistances in that track. These lock the BIT in either of its loaded or released configurations. (b) The BION is released/unsheathed by the gunbolt action of the peg, which withdraws the cannula from over the probe and BION, while these both remain in position. (c) The BION is loaded into the distal cannula to abut against the probe tip, and is secured by opposing dimple indents from the cannula wall. The BION's electrodes contact body fluids via the cannula's conduction holes and distal opening. Designs prepared using Autodesk Inventor™ (Autodesk Inc., San Rafael, CA).

produced by the Alfred Mann Institute for Biomedical Engineering at the University of Southern California (AMI-USC), and has been used successfully for over 30 BION implants in human subjects to date.

Previous BION Implantation Method and Concerns

Prior to the BIT, clinical implantation of BIONs was carried out using a modified intravenous drip set

(Angiocath™, BD Medical, Franklin Lakes, NJ). Electrical stimulation was used to identify the ideal location for the BION, via the tip of an otherwise insulated 17G needle that constituted a sharp, stiff trocar within a 12G, soft plastic sheath that provided a cannula. The needle was then withdrawn to leave the plastic cannula *in situ*. The BION was manually inserted into the cannula and extruded from the distal end with the help of a pushrod. The cannula and



FIGURE 2. The BIT loaded with a BION, in sterile packaging ready for shipping. Note the window cut-out in the cardboard tray beneath the BION chamber, to allow functional testing after packaging and sterilization.

pushrod were then removed. Concerns with this technique included: exposure of the BION to handling risks and potential for damage and contamination; drift from the implantation site during handling and extrusion; difficulty delivering the implant through an upward directed cannula; inability to predetermine the implant's axial orientation; and perhaps most important, the inability to test the BION *in situ* prior to release. The BIT described here was designed to address all of these issues.

Design Requirements

- (1) Minimal tissue trauma
- (2) Small profile (no bigger than the 12G tool previously used)
- (3) Accurate localization (via electrical stimulation and/or radiologic screening)
- (4) Complete protection of the implant throughout delivery
- (5) Functional testing *in situ*, in real-time throughout delivery
- (6) Retrieval of implant at any point prior to release
- (7) Ability to inject or withdraw fluids at tool tip
- (8) Control of axial orientation at delivery (important for implants containing motion sensors)
- (9) Simple and intuitive operation
- (10) Operable in any position or orientation
- (11) Minimal handling of the BION during implantation
- (12) Biocompatible materials for brief contact with tissue
- (13) Sterilizable by steam autoclave (current validated method for BION implants), or gas, e.g., ethylene oxide (ETO) for mass production

Strategy

Hypodermic needles that become disabled automatically after use are being developed to avoid the

hazards of unsterile re-use and accidental needle-stick injury.^{3,9,17} One approach is to use thermoplastic polymers instead of metal because they can be dulled and sealed by applying moderate heat. Because plastic needles buckle more easily than metal ones, the development of such needles to date has been limited to applications that require short, fine needles, such as for immunization programs and insulin delivery, e.g., 12.7 mm (0.5") length \times 22G (OD 0.7 mm (0.028"), ID 0.4 mm (0.016")).⁸ The BIT requires a much larger gauge (OD 2.8 mm (0.110"), ID 2.2 mm (0.085") = 12G) and shank length (100.0 mm to reach deep muscles), posing various challenges for design and fabrication.

The main decision was to deliver the BION implants preloaded into the tool from which they would be released. The BION itself would then generate the trial stimulation pulses required to determine its location by physiological monitoring of the evoked response (e.g., visible or palpable muscle twitch or electrophysiologically recorded M-wave). For this to work, the tool must not interfere with the RF magnetic field that powers and controls the implant, and it must not block or short the stimulation pulses that it generates from passing through the target tissue outside the tool. These secondary requirements, in turn, mandate the use of electrically and magnetically non-interfering materials (non-conductive and non-ferrous), plus fenestrations to permit egress of stimulation currents. Those materials must then provide the strength, biocompatibility and manufacturability to achieve the rest of the requirements. With suitable materials in hand, the rest of the design could focus on the ergonomics of loading and stabilizing the implant and releasing it precisely at the target site, which is described first to orient the reader to the mechanical analysis that follows.

The BIT has two main parts that move relative to each other to release the implant: a plastic cannula with a sharpened tip, and a probe within the cannula behind the BION (Fig. 1). The probe is attached to the main body of the handle so that the operator naturally tends to stabilize this part of the tool with respect to the target site. The cannula is attached to a gun-bolt-like assembly within the handle that allows it to be withdrawn over the probe and implant to effect release. After assembly of the BIT, the BION is loaded via the distal end of the cannula so that its Ir electrode abuts the probe tip and its Ta electrode (effective cathode for stimulation pulses) lies exposed just within the bevel of the needle. The BION is retained in this loaded position and axial orientation by friction between its glass capsule and two opposing dimple indents created by mechanically deforming the walls of the cannula (Fig. 1c). The BION's axial orientation is set at loading relative to the cannula handle peg position (taking into

account the 90° axial role that will be associated with deployment), so that the clinician is able to orient the BION axially as desired at insertion. The cannula's sharp tip is double-beveled to minimize the stress of implantation. The loaded BION-BIT is secured in a customized cardboard tray, which has a window cut-out beneath the BION chamber for functional testing after packaging and sterilization (Fig. 2). We have determined previously that the voltage change produced on the electrodes in air when a stimulation command is received can be detected by capacitive coupling to electrodes that are sufficiently close (<2.0 mm). The entire assembly is sealed in a Tyvek™ pouch, sterilized and delivered for implantation as a single unit.

METHODS

Needle Tip Stress Profile

In order to choose an appropriate material for the BIT cannula, we needed to ascertain the forces that it would have to withstand at its tip during insertion and movement through muscle. A stainless ~12G steel tube (OD 2.8 mm (0.110"), ID 2.0 mm (0.080")) was fashioned into a needle with a double-beveled tip. Two strain gauges (BLH SR-4®; Vishay Micro-Measurements, Raleigh, NC) were recessed onto opposite sides of the needle tip, and their connections brought out through the proximal end of the needle to an amplified Wheatstone bridge configuration (LM6132 dual operational amplifier; National Semiconductor, Santa Clara, CA). The system was calibrated using a force gauge (FG-5000; Extech Instruments, Waltham, MA) to exert lateral bending tip forces; it exhibited a linear output relationship up to 6.4 N. The needle was used to measure lateral forces during four repetitions of

each of the following five use-cases in a large block of porcine muscle: (1) inserting through fascia; (2) traversing parallel to muscle fibers; (3) traversing transverse to muscle fibers; (4) hitting up against bone with reasonable surgical caution; (5) hitting up against bone vigorously and recklessly (Fig. 3). The average *peak* force experienced by the tip was determined for each use-case.

Wall Thickness Requirements and Material

In order to determine an appropriate polymeric material and wall thickness for the BIT, a flexural stiffness was required that would be sufficiently strong (as determined by the section "Needle Tip Stress Profile" above), and yet would still provide similar handling characteristics as our original insertion tool. The stiffness of the prior tool, based on the 12G Angiocath unit, was attributable largely to the 17G stainless steel needle that formed a core within the soft polymeric sheath. Therefore the aim for the BIT was to achieve at least the same desired handling characteristics and safety in bending as such a 17G stainless steel needle. The outside dimension (OD) of the BIT cannula was limited by the 12G OD requirement (=2.8 mm (0.110")), and the inside dimension (ID) had to be sufficient to clear the OD of the implant (=2.2 mm (0.085")). The required minimal flexural modulus for a material that would form the BIT cannula was computed as follows.

Basic stiffness equation for a cylinder in bending (supported at both ends; single load in center)¹²:

$$\delta = \frac{PL^3}{48EI} \quad \text{and} \quad I = \frac{\pi}{64}(D_o^4 - D_i^4)$$

where δ = maximum deflection (m), P = load (N), L = length (m), E = Young's modulus of elasticity

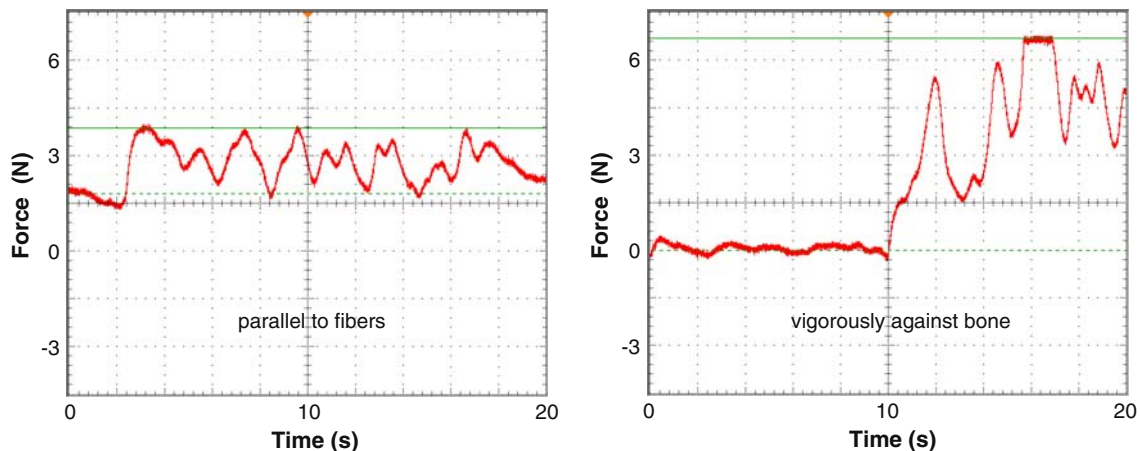


FIGURE 3. Needle tip stress profiles measured traversing parallel to muscle fibers (left) and hitting vigorously against bone (right).

(N m^{-2} or Pa), I = area moment of inertia (m^4), D_o = outer diameter (m), and D_i = inner diameter (m).

To achieve the same desired stiffness coefficient (represented by P/δ (N m^{-1}), i.e., the force required to produce a unit displacement) for both the given stainless steel “S” cylinder at 17G and our desired material “M” cylinder at 12G:

$$\frac{P_S}{\delta_S} = \frac{P_M}{\delta_M}$$

So that ultimately:

$$E_M = E_S \frac{D_{So}^4 - D_{Si}^4}{D_{Mo}^4 - D_{Mi}^4}$$

The ID that will accommodate the implant and the OD that is required are both fixed (D_{Mi} , D_{Mo}), and the remaining variables are given for the stainless steel device (E_S , D_{So} , D_{Si}). Thus we can determine the requisite minimal flexural modulus for a material (E_M), to form a BIT cannula with the same desired stiffness as our prior stainless steel version.

Selection and validation of the final material was an iterative process, involving a systematic search based on the formalized requirements. The final polymer selected was a 30% glass reinforced liquid crystal polymer (Vectra™ B130; Ticona, Florence, KY). The models and experimental results described below are for this material.

Conduction Hole Size and Configuration Experiments

Holes in the wall of the cannula are desirable for three reasons: (1) to provide conduits so that the Ir electrodes of the BION become bathed with tissue fluids to allow testing during implantation; (2) to act as rule marks (10.0 mm intervals) to keep track of insertion depth; and (3) to permit ingress of steam or gas used to sterilize the less accessible regions of the loaded BIT. The following studies were used to ascertain the optimal size, number, and configuration of holes that would meet these needs but not compromise adequate cannula wall strength:

Adequacy of Conduction Holes

The stimulus output circuitry of the BION generates current-regulated pulses over the range 0.5–31.5 mA with an available compliance voltage of 14 V. The actual output current that it can produce will be limited by the total load impedance (electrodes plus surrounding fluid and tissue) according to Ohm’s law. Experience has shown that it is useful for clinicians to be able to apply test stimulus pulses of up to 10 mA at least initially while searching for the desired low-threshold target (typically around 1 mA). The 10 mA

pulse can be delivered only if the load impedance is below 1.4 k Ω when the BION is in the BIT. Rather than measure the actual load impedance, we instead measured the requested stimulus current at which the amplitude of the electrical field created in the surrounding tissue ceased to increase (indicating that the compliance voltage had been reached). We measured the maximal output current obtained from BIONs within Vectra cannulae with different size holes (\varnothing 0.9 mm (0.035”) or \varnothing 1.3 mm (0.050”)), in both single hole and double hole (through-&-through, i.e., through both walls) configurations; each inserted into porcine muscle, muscle-saline (muscle immersed in saline), and saline (Fig. 4 demonstrates an example of the normal BION characterization test compared to the worst case experimental scenario, i.e., in muscle without saline).

Cannula Breaking Strength

The worst case scenario based on geometry would be that in which the cannula is fixed just proximal to the conduction holes and then loaded laterally at its tip. This represents the condition where the cannula is largely inserted into the muscle, supported by the surrounding tissues, and the tip hits a bony resistance. This would result in bending and perhaps failure just where the wall is weakened by the conduction holes. This experiment was therefore performed on 30.0 mm lengths of 12G Vectra cannula, with the same permutations of holes as described in the section “[Adequacy of Conduction Holes](#)” above. The hole(s) were drilled 20.0 mm from the tip, and the cannulae were fixed in a vice 2.0 mm proximal to them, to leave 22.0 mm exposed shank length. Breaking tests were performed by loading the free tip of each sample with a force gauge (FG-5000; Exttech Instruments, Waltham, MA), in orthogonal axes and in both directions for the asymmetrical single-hole design. For each possible configuration 3 tests were run, from which the average breaking force was determined, and the failure modes (whether the samples broke or buckled) were recorded.

Sterilization Validation

Assembled and packaged BITs with BIONs were tested in order to validate that the various openings designed into the cannula actually do offer sufficient access for steam sterilization. Five cleaned BION–BIT assemblies were inoculated with 10^6 microorganisms (*Geobacillus stearothermophilus*; STS Life Sciences, Ethox International, Rush, NY), in the most problematic locations on both the middle of the BION and the middle of the probe inside the cannula. All were packaged and sealed. One sample was left unsterilized as a control; 2 were autoclaved for a half-cycle

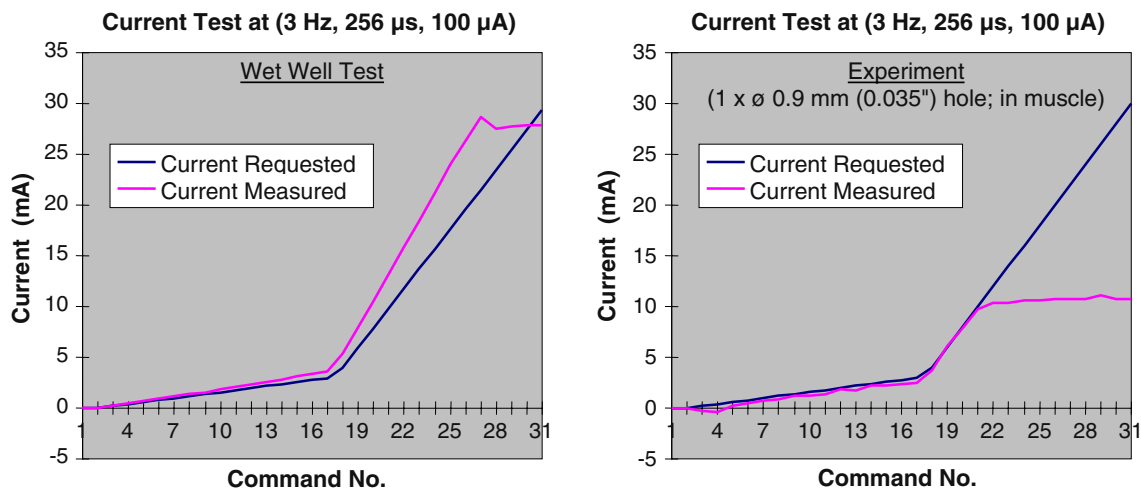


FIGURE 4. The BION Wet Well Test (left) characterizes a BIONs normal function: the command no. requests successively higher current output (blue), and the BIONs response is measured as current delivered (magenta). In the worst case experimental scenario (right), we see that even with only a single small \varnothing 0.9 mm (0.035") hole in muscle, the BIONs maximum deliverable current is still adequate at 11 mA (see text).

(250 °F \times 17 min); and 2 were autoclaved for a full-cycle (250 °F \times 35 min). Each BIT was then dismantled and spore retrievals were cultured. Sterilization was considered adequate for samples that yielded no viable spores while the control sample yielded viable spores. In order to be sure that repeated sterilization would not damage either the BIONs or the BITs, assembled sets were subjected to three repeated autoclave cycles at twice the full-cycle duration. Then the BIONs were characterized for their full range of stimulus output parameters; and the BITs were tested for changes in average dimensions, breaking strength, and handling properties (surface texture, flexibility, friction between parts, and locking and unlocking of handles during loading and releasing).

Finite Element Analysis of Lateral Bending Strength and Buckling Strength

A 3D FEA model of a cannula was developed in MSC.AFEA™ (MSC.Software, Santa Ana, CA), to estimate (1) bending strength on lateral loading at the tip; and (2) buckling strength on axial loading. Various combinations of materials, dimensions (wall thickness, gauge and length), and conduction hole configurations (size, number and position) were simulated. The model was validated in three ways: (1) observation of multiple simulations under different configurations during which it behaved intuitively and qualitatively similar to the physical object; (2) comparison of model data during simulations to analytical solutions of idealized structures; and (3) comparison of simulation results with data obtained experimentally during identical

standardized loading on the bench. MSC.Marc was used as the FEA solver and MSC.Patran as the pre- and postprocessor. For accuracy the analyses were limited to small deformations, and so the Vectra polymer was modeled as isotropic/linear elastic with the following material properties: Young's modulus $E = 2E10 \text{ N m}^{-2}$ (Pa), Poisson's ratio $\mu = 0.4$, and mass density $\rho = 1.6E3 \text{ kg m}^{-3}$. A uniform mesh of quadrangular elements was used, limited to the 500 element educational version of the software.

Lateral Tip Loading

Model

The worst case scenario was modeled: boundary conditions were set for cantilever bending with the cannula fixed just proximal to the conduction holes and then loaded at its tip 22.0 mm distally and perpendicular to its long axis. As described in the section "[Cannula Breaking Strength](#)" above, this represents the condition where the cannula is largely inserted into the muscle, supported by the surrounding tissues, and the tip hits a bony resistance causing bending just where the wall is weakened by the conduction holes. The load was applied at a point and ramped up over 1 s. Analyses were run as non-linear, static, 3D, solving for large displacements/large strains with an updated Lagrangian scheme, and using the full Newton–Raphson iteration method.^{2,4} In calculus this method is often referred to as Newton's method for extracting a root of a polynomial. Since the strains are nonlinear functions of the displacements, the stiffness is dependent

on the displacements. Therefore, the solution of the displacements cannot be obtained in a single step, and so a series of increments are combined with iterative equilibrium corrections at every step.

Theoretical

Using the Euler–Bernoulli beam equation¹²:

$$\sigma_{\max} = \frac{M_b r_o}{I}$$

where σ_{\max} = bending stress (N m⁻² or Pa), M_b = bending moment at the neutral axis (N m), r_o = outer radius, i.e., perpendicular distance to the neutral axis (m), and I = area moment of inertia about the neutral axis (m⁴).

$$M_b = F \times \ell$$

where F = tip bending force (N), and ℓ = length (m).

$$I = \frac{\Pi}{4}(r_o^4 - r_i^4)$$

for a cylinder (as above).

Experimental

Standardized lateral tip loading tests of this same worst case scenario were performed in the section “[Cannula Breaking Strength](#)” above, and the results compared with the model and theoretical data derived above.

Axial Loading

Model

A 100.0 mm length of cannula was modeled for axial buckling, with and without $2 \times \emptyset 1.3$ mm (0.050”) through-&-through holes 20.0 mm from the distal end. Boundary conditions were set as clamped-guided (proximal-distal). The buckling analysis was performed with a static linear compression step (small displacements and strains), and by the full Newton–Raphson iteration method, with a Lanczos eigenvalue extraction scheme to derive the critical buckling load P_{cr} (N) from the eigenvalue EV and the applied load $P_{applied}$ (N):

$$P_{cr} = EV \times P_{applied}$$

Theoretical

Using Euler’s buckling formula¹²:

$$P_{cr} = \frac{\Pi^2 EI}{L^2}$$

where E = Young’s modulus of elasticity (N m⁻² or Pa), I = area moment of inertia of the cross-section

(m⁴), and L' = effective length of the cylinder (m), which depends on the boundary conditions:

$$L' = \frac{L}{\sqrt{C}}$$

where C is a function of end constraint (for clamped-guided $C = 1.0$).

$$I = \frac{\Pi}{4}(r_o^4 - r_i^4)$$

for a cylinder (as above).

Experimental

Cannulae were tested on the bench for axial loading in order to: (1) characterize cannula buckling behavior under uniaxial compression, thus simulating conditions similar to those encountered during insertion through the fascia; and (2) derive data for comparison with our FEA simulations and theoretical calculations above, in order to validate these. Buckling tests were performed on 10 lengths of extruded and post-processed 12G Vectra cannula, each 100.0 mm long, OD = 2.8 mm (0.110”), ID = 2.2 mm (0.085”). To mimic our modeling and theoretical calculations, five samples had no holes drilled (the “no-hole” group) and 5 had $2 \times \emptyset 1.3$ mm (0.050”) through-&-through holes drilled 20.0 mm from one end, termed the “distal end” (the “hole” group). The failure modes, critical buckling loads and critical failure loads were determined for each of the two groups (hole group shown in Fig. 5); and these were compared with model and theoretical data for the same scenarios. Testing was performed using an Instron[®] 5567 Load Frame running Bluehill[®] 2 Software (Instron, Norwood, MA), compression speed 20 $\mu\text{m s}^{-1}$, displacement stroke ~ 1 μm , 30 kN capacity load cell (accuracy $\pm 1\%$ at 10 N) mounted to actuator head, sampling at 20 Hz. Each specimen was mounted precisely vertically using a V-block. The load

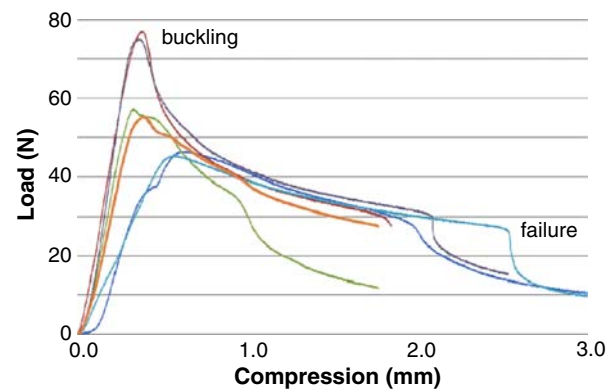


FIGURE 5. Buckling analysis results for samples with holes. Average shown in bold. Example buckling and failure points are indicated.

response was recorded as a function of uniaxial compressive displacement through buckling in all samples, and until the specimens failed (kinked or broke) in nine samples (the first sample could not be run to failure as it was used to test the set-up and subjectively assess the behavior: this sample was run at the machine's current default setting for termination at 40% of maximal load, which was reached without failure; all subsequent specimens were run to 20% of maximal load and all ultimately failed). Buckling was assumed to occur at the maximal recorded load for each sample. Failure was assumed to occur at the sudden drop in loading force after buckling (Fig. 5).

RESULTS

Needle Tip Stress Profile

Figure 3 shows examples of measurements of force experienced by the tip of a 12G needle. In this way the average *peak* forces for each of the following five use-cases were found to be: (1) inserting through fascia = 4.2 ± 0.2 N (3.9–4.4); (2) traversing parallel to muscle fibers = 0.9 ± 0.1 N (0.8–1.0); (3) traversing transverse to muscle fibers = 4.9 ± 0.1 N (4.8–5.0); (4) hitting bone with reasonable surgical caution = 5.3 ± 0.2 N (5.1–5.5); and (5) hitting bone vigorously = $>7.3 \pm 0.0$ N (7.3–7.3; this fell within the early non-linear portion of the system's force–voltage relationship). It is recognized that as each of these values is the average of the *peaks* of only four similar runs, the ranges are narrow and the standard deviations are small. It was thus ascertained that a 12G needle of a non-metal material must also be able to withstand at least these forces under these same conditions.

Wall Thickness Requirements and Material

The minimal flexural modulus for a material to form a BIT cannula with the same desired stiffness as our prior stainless steel version was found to be 18.0 GPa. A variety of materials that met this specification were considered for their appropriateness to our other design requirements (see [Discussion](#)). The final two were: (1) a 55% glass reinforced thermoplastic polyester resin of modified PET (polyethylene terephthalate) with $E = 17.9$ GPa (Rynite™ 555; DuPont, Wilmington, DE); and (2) a 30% glass reinforced liquid crystal polymer with $E = 20.0$ GPa (Vectra™ B130; Ticona, Florence, KY). Vectra was ultimately selected for its preferred flexural modulus as well as a variety of other design considerations discussed below.

Conduction Hole Size and Configuration Experiments

Adequacy of Conduction Holes

As expected, the results were spread across a spectrum from the worst obtained with a single smaller hole in muscle (Fig. 4), to the best obtained with larger double holes in saline. All configurations met the 10 mA requirement, however, so the design of the holes was based on the results of studies “[Cannula Breaking Strength](#)” and “[Sterilization Validation](#)” below.

Cannula Breaking Strength

By comparing breaking strengths with the known tip forces that the cannula must be able to withstand (as per the section “[Needle Tip Stress Profile](#)” above), it was found that $2 \times \varnothing 0.9$ mm (0.035”) holes would offer sufficient strength, while still allowing adequate conduction as per the section “[Adequacy of Conduction Holes](#)” above. In the case of the $2 \times \varnothing 1.3$ mm (0.050”) hole samples, the average breaking strengths were 9.9 ± 4.5 N (5.0–14.1) for lateral tip forces exerted perpendicular to the axis of the holes, and 8.1 ± 0.7 N (7.3–8.7) for lateral tip forces exerted parallel to the axis of the holes (this is of relevance to validating our FEA model described in the section “[Finite Element Analysis of Lateral Bending Strength and Buckling Strength](#)” below). Whether the failure mode consisted of buckling or breaking appeared to be uncorrelated with hole pattern or loading direction.

Sterilization Validation

After spore retrieval, positive cultures were found on all sites of the control sample and on all sites of the half-cycle samples (250 °F \times 17 min). Negative cultures were found on all sites of the full-cycle samples (250 °F \times 35 min). This effective kill cycle was doubled to determine a final standard autoclave protocol of 250 °F \times 70 min. Both the BION and the BIT were shown to adequately withstand this sterilization for three cycles without degradation of their mechanical, electrical or biomaterial properties.

Finite Element Analysis of Lateral Bending Strength and Buckling Strength

Lateral Tip Loading

Model

In the model without holes, a lateral tip load of 5.0 N generated a maximal tensile stress $\sigma_{\max} = 90E6$ N m⁻² at the fixed end. When $2 \times \varnothing 1.3$ mm (0.050”) holes were added 20.0 mm from the tip (2.0 mm from the fixed end), for the same loading conditions: the maximal tensile stress increased to $110E6$ N m⁻² when the tip

load was applied *perpendicular* to the axis of the holes; and to $126\text{E}6 \text{ N m}^{-2}$ when applied *parallel* to the axis of the holes. The model confirms that holes increase the risk of failure, particularly for forces parallel to their axis. In order to compute the forces at which the cannulae would break, Vectra was assumed to be non-deformable/non-plastic with a linear stress:force relationship until breaking. For each scenario the results were extrapolated until the maximal tensile stress exceeded the published tensile breaking stress = $205\text{E}6 \text{ N m}^{-2}$ (Vectra™ B130 datasheet; Ticona, Florence, KY). The cannula was projected to break at 9.4 N (= $207\text{E}6 \text{ N m}^{-2}$ tensile stress) for perpendicular stress, and at 8.2 N (= $207\text{E}6 \text{ N m}^{-2}$ tensile stress) for parallel stress.

Theoretical

Using the Euler–Bernoulli beam equation with actual BIT parameter values for the no-hole scenario described in the model above, the calculated $\sigma_{\text{max}} = 80\text{E}6 \text{ N m}^{-2}$, in reasonable agreement with $90\text{E}6 \text{ N m}^{-2}$ predicted by FEA above.

Experimental

As per the section “**Cannula Breaking Strength**” above: with $2 \times \varnothing 1.3 \text{ mm}$ (0.050”) holes the average breaking strengths found experimentally were 9.9 N for tip forces exerted perpendicular to the axis of the holes, and 8.1 N for tip forces exerted parallel to it. The model accurately predicts similar values for these scenarios at 9.4 and 8.2 N , respectively (above), confirming our assumption that the stress:force relationship for Vectra is linear until the cannula breaks.

Axial Loading

Model

In samples without holes, for a unit compression load, the model gives an $EV = 39.4$, representing a buckling load of 39.4 N , with a lateral displacement of 24.6 mm . The addition of $2 \times \varnothing 1.3 \text{ mm}$ (0.050”) through-&-through holes 20.0 mm from the distal end results in an $EV = 38.6$, representing a reduced buckling load of 38.6 N , with a slight increase in lateral displacement to 24.7 mm .

Theoretical

Using Euler’s buckling formula for a no-hole cylinder, calculated $P_{\text{cr}} = 38.0 \text{ N}$, matching the model’s 39.4 N simulation value closely (within 4%).

Experimental

Failure Modes: Of the 9 specimens run to failure, only one “hole” specimen broke (fractured through its

holes). All other failures in both no-hole and hole groups were by buckling. All failures occurred at widely varying locations in all specimens; in the hole group none were related to the holes in either position or axial orientation.

Critical Buckling Loads: Mean critical buckling load for all samples was $55.3 \pm 13.7 \text{ N}$, at a compression of $0.6 \pm 0.3 \text{ mm}$. The critical buckling loads fell within a wide range (39.4 – 77.0 N), the minimum of which correlates well with our model predictions and theoretical calculations above. For the small number of samples tested, there was no significant difference between the cannulae with and without holes.

Critical Failure Loads: After buckling, failure occurred at a mean load for all samples of $27.8 \pm 4.4 \text{ N}$, over a much narrower load range than for buckling (22.5 – 34.7 N), but at more widely varying degrees of compression ($2.4 \pm 1.1 \text{ mm}$). For the small number of samples tested, there was no significant difference between the cannulae with and without holes.

DISCUSSION

Material Selection

Materials have been selected so as to ensure that the combined instrument meets the design requirements, particularly regarding strength, sharpness, biocompatibility, sterilization and electrical resistance. Of all the parts, the cannula’s properties are the most crucial, both mechanically so that it withstands insertion stresses and strains, and electromagnetically so that it does not interfere with the BIONs function as a microstimulator. The cannula also must undergo critical fabrication steps to produce its sharp, beveled tip, perforations and indentations.

We have calculated that a 12G cannula with a wall-thickness of 0.32 mm (0.0125”) will have the same flexural strength as a standard 17G stainless steel needle if it is made from a material with a flexural modulus of at least 18.0 GPa . To obtain this high degree of stiffness, a polymeric material generally requires longitudinal fiber filling (e.g., carbon or glass). Filled plastics are generally more suited to injection molding than extrusion, but extrusion is more desirable for the thin-walled cannula. The cannula material must also be non-ferrous and sufficiently non-conductive (such that it does not permit eddy currents), so as not to distort the electromagnetic field used to power the implant for testing it while it is still housed within the cannula. The material’s resistivity must therefore be at least greater than that of body tissues ($\sim 1 \Omega \text{ m}$). The polymer should also be impact resistant and suited to sterilization, e.g., autoclaving (softening temperature must exceed $250 \text{ }^\circ\text{F}$) or ETO (ethylene oxide) gas sterilization for mass production.

Based on these considerations, Vectra™ B130 was chosen for the cannula (30% glass-filled liquid crystal polymer, black; Ticona, Florence, KY). Vectra can be molded or extruded. For cannula production it is simultaneously drawn and extruded (Precision Extrusion, Glens Falls, NY). The raw stock is then post-processed by the manufacturer in a solid state polymerization process. After extrusion the cannulae are re-heated and held at the curing temperature during which time the polymers further cross-link, resulting in increases in molecular weight, melt temperature, tensile strength (up to 50%) and flexural modulus (up to 50–100%). The process results in cannulae that fail less easily, tend to kink rather than fracture, and are left with a smooth, even and shiny outer surface. This polished outer surface minimizes drag through the tissues, while the luminal surface is adequately suited to movement over the probe and BION. Afterward the through-&-through conduction and depth-marking holes, and the beveled tip, are laser cut (Accu-Met Laser, Cranston, RI). Laser cutting leaves smooth, precisely formed features (accuracy to 0.025 mm (0.001")). The highly localized heat flashes the edges, fusing them and leaving no torn or loose glass fibers exposed from the sealed polymer, as would occur with drilling or machine cutting. Compared with conventional machining, this method is also more accurate, repeatable, and time and cost efficient. The size of the electrical conduction openings has been determined to allow adequate exposure of the electrodes to body fluids, while still maintaining sufficient strength for even a clumsy insertion. Finally, the two opposing dimple indents are made to hold the BION. First a small hole is created with a dental pick at each site, and then a customized 25.4 mm (1") micrometer is screwed 0.9 mm (0.035") into the cannula wall at those points. This leaves opposing detents of ~0.6 mm (0.025") each, protruding into the cannula's lumen and against which the BION is loaded. If reloading of a BION is required during assembly, these dimples are cleared with a 2.2 mm (0.085") calibration pin, and recreated at another point on the cannula's circumference. This method is not particularly precise but it can be used reliably to produce friction forces in the broadly acceptable range of 0.5–5 N. A calibrated tool is used for loading the BION into the distal end of the BIT so that an acceptable holding force can be verified. Packaged BION–BIT assemblies were tested in 6 cross-country flights to ensure that they were not damaged or dislodged by normal air freight/postal handling.

Buckling analysis of the cannula has revealed that: (1) relative to the critical buckling loads found experimentally, the FEA model and theoretical calculations provide conservative results, offering a margin of safety; and (2) the cannulae will fail at their weakest

point, which is unrelated to the presence, position or axial orientation of holes. The mean critical buckling load (~55 N) exceeds the model/calculated data (~39 N) by about 41%. This is in keeping with: (1) the post-processing which stiffens the cannulae and increases their resistance to buckling by up to 50%, which is not accounted for in our model/calculations; and (2) the manufacturing technique whereby the cannulae are simultaneously drawn and extruded, with resultant anisotropy of the glass fibers that may also alter resistance to buckling. The critical failure loads were found to occur at widely varying degrees of compression, and at widely varying locations. Therefore, if failure is occurring at the walls' weakest points, these points must occur randomly in location and degree. Although the cannulae look smooth and polished on the outer surface as the result of post-processing, it is believed that these random weakest points result from irregularities in the wall thickness due to the extrusion process and fiber filling. At a microscopic level this can be seen as longitudinal irregularities up to 0.19 mm (0.0075") deep on the inner/luminal surface (Fig. 6a), which are random and significant (60%) relative to the overall wall thickness of 0.32 mm (0.0125"). On a macroscopic level the internal wall thickness can also be seen to vary

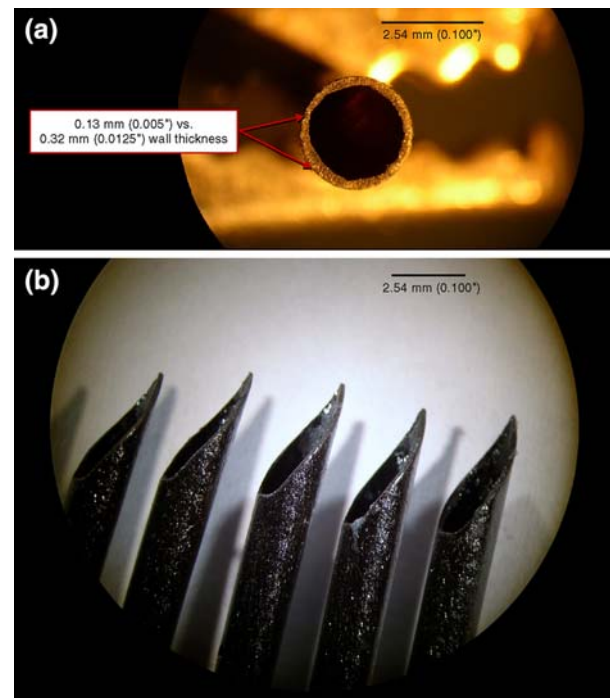


FIGURE 6. Light micrographs of cannulae: (a) Representative section detailing cannula wall thickness variations down to 40% of desired thickness (11× magnification). (b) Sharpened tips of five cannulae, before and after a progressively increasing number of random passes through a slab of porcine muscle with thick fascia: 0, 1, 3, 10, and 30 passes from L to R respectively (8× magnification).

somewhat as gentle undulations along its length (most likely due to subtle variations in the drawing speed during extrusion).

The mean critical buckling load was compared to anticipated axial insertion forces for a needle in soft tissue. Studies have shown that the axial load on a needle during insertion into soft tissue is the summation of different forces distributed along the needle shaft (cutting force, friction force and stiffness force), and that these forces can be modeled as functions of position (x) of the needle tip during insertion, to obtain results comparable with experimental data^{1,5,14}:

$$f_{\text{needle}}(x) = f_{\text{cutting}}(x) + f_{\text{friction}}(x) + f_{\text{stiffness}}(x)$$

Values for axial insertion forces range from ~1.45 N required to puncture liver capsule for example (analogous to fascia), up to ~14 N to puncture skin *in vivo*, with most published values falling in the 3–5 N range for needles with a ~22° bevel (the BIT bevel is 25°).^{13,14} The BIT is designed to be implanted via a stab incision through the skin, so the largest axial forces should arise from penetrating fascia (1–3 N range). Even if it were used to puncture skin directly, the ~55 N mean critical buckling load provides a safety factor of four-fold over the worst case puncture force of ~14 N anticipated during implantation. Furthermore, in all but one instance, the cannulae were found to kink rather than fracture. This failure mode (large scale plastic deformation) presents less of a hazard than the catastrophic failures associated with buckling in more brittle materials. Also of interest was how resilient the sharpened tip features would remain under these types of loading. Figure 6b shows the magnified tips of 5 cannulae, before and after a progressively increasing number of random passes through a slab of porcine muscle with thick fascia (0, 1, 3, 10, and 30 passes). At 8× magnification the tip features remained visibly unaltered in all cases.

The role of FEA in the cannula development was threefold: (1) Modeling indicated that the empirical experimental results were consistent with expectations, as opposed to reflecting a random state of poorly controlled variables such as wall thickness and uniformity. (2) Modeling predicted that it should not be necessary to include a probe or a BION within the cannula for testing, as the amount of deflection of the cannula wall before it started to fail catastrophically should not exceed clearance to the implant nor the flexible probe. This was important so that the implant would not be taking up any significant stress during insertion; and because these components would therefore be unlikely to produce mechanical stress risers at the probe/BION junction that could otherwise cause mechanical failures at lower force levels than

were predicted. Experimental findings also confirmed that the failures occurred more proximally than where the BION would have been, i.e., where the bending stresses were higher. (3) The validated FEA model will be useful for future designs/other possible variants of the BIT.

The materials used for the remaining parts of the instrument are less critical. We chose to make the prototypes described herein by machining and joining of relatively simple components. The component designs and materials are suitable for injection molding, which would greatly reduce unit costs for mass production:

- *cannula handle and peg*: polyetherimide (Ultem™, amber; SABIC Innovative Plastics, Pittsfield, MA);
- *probe*: polycarbonate (Makrolon™, clear/white; Bayer MaterialScience, Pittsburgh, PA);
- *probe handle*: carbon-filled PEEK (polyetheretherketone, black; McMaster-Carr, Atlanta, GA).

The probe's 21G central lumen, in addition to providing injection/aspiration functionality to the BIT, also facilitates better extrusion tolerances by allowing degassing during manufacture. Its clear color contrasts with the black cannula to enhance the visibility of the depth-marking holes. All materials chosen interact with each another and the cannula in a predictable fashion to meet the design requirements, e.g., to provide sufficient stiffness, predictable locking and unlocking forces, friction and/or frictionless movements as required between parts and within tissues, etc. Further, they can easily be fused together using cyanoacrylate glue if necessary. They are also already in use commercially for other medical applications such as in laparoscope handles.

Preimplantation and Prerelease Testing

The two electrical conduction openings adjacent to the BIONs Ir electrode (Fig. 1c), together with the cannula's terminal opening adjacent to the Ta electrode, facilitate repeated stimulation at any point while traversing the tissue path so as to determine the desired implant location. Both the function of the implant and the accuracy of its placement can be confirmed before release. More systematic testing of incremental recruitment of the muscle can be obtained by recording and measuring the M-wave produced by stimulus pulses of varying intensity above threshold. The M-wave is the electrical potential produced by the synchronous activity of those muscle fibers innervated by the stimulated motor axons. The M-wave can be recorded from the skin surface or via an intramuscular EMG needle electrode. The digitized M-wave data can

be used by a computer program to continuously adjust the stimulus level to stay near threshold and to provide information about this threshold intensity via audio feedback to the operator. This seems likely to speed the insertion procedure and minimize the need for a technically proficient assistant. The growth of the M-wave can provide important information about the location relative to the nerve and its intramuscular branches.¹⁶

Implantation

General surgical principals teach the implantation of all foreign bodies by sterile, non-touch techniques. To that end, the transmission coil is either set up preoperatively around but not contaminating the surgical field, or draped in a sterile see-through bag and brought into the surgical field as required. In the former case, the insertion site is prepared preoperatively with antiseptic wash, the coil is placed around the perimeter of the insertion site, and the full area (including the coil) is draped with a sterile, adhesive polyurethane film, e.g., OpSite™ (Smith & Nephew, Largo, FL) or Steri-Drape™ (3M, St. Paul, MN). To minimize trauma, an EMG stimulating needle electrode (21G = \varnothing ~0.8 mm (0.031") insulated may be used to locate an optimal point of stimulation before the larger BIT is introduced. The BIT has a large V-shaped 45° groove (Fig. 1), aligned through both handles in the loaded configuration, so that it may be guided over and parallel to this stimulating electrode. Alternatively, the physician may prefer to use the EMG electrode to locate the motor point by the most direct route according to surface landmarks, even if this is perpendicular to the target nerve. The BION is then implanted from a more distant location by triangulating toward the EMG electrode tip as a guide. In this way the BION can more likely be oriented parallel to the nerve and fascial planes, where it is less likely to experience motion or changes in recruitment properties during muscle activation or postural shifts.

Clinical Experience

Over the course of a year, both the BIT and the prior insertion apparatus were made available for implants. At the discretion of the clinicians, of 33 BIONs requiring implantation by injection, 30 BIONs in 16 patients were implanted using BITs. Three BIONs in 2 patients were implanted using the prior apparatus that permitted test stimuli to be applied through its removable trocar because in these cases the external RF-coil was unable to activate the BIONs in the surgical field. In general, the clinicians found the BIT preferable because it was simple, intuitive and easy to use, facilitating rapid and accurate placement.

CONCLUSIONS

The polymeric BIT described here takes advantage of very stiff, filled polymers, and laser fabrication techniques that have only recently been developed. This permitted the design of a relatively large, long, strong and sharp needle-like tool that was both electrically non-conductive and electromagnetically inert (unique requirements for this particular application). The design, materials and validated analytical techniques can be readily adapted for other applications where such properties may be desirable, e.g., drug implants, chemotherapeutic agents, transplanted tissues and cell cultures, radiotherapeutic beads, etc. The friction fit and release mechanisms helped provide a simple, low-cost design that is easy and intuitive to use.

ELECTRONIC SUPPLEMENTARY MATERIAL

The online version of this article (doi:[10.1007/s10439-009-9739-5](https://doi.org/10.1007/s10439-009-9739-5)) contains supplementary material, which is available to authorized users.

ACKNOWLEDGMENTS

Contributions to this research were made by Ray Peck and Jasspreet Singh (AMI-USC, technical advice and prototyping); Rahman Davoodi (AMI-USC, modeling); and Warren G. Haby (USC Department of Mechanical Engineering, buckling tests). All are from the University of Southern California, Los Angeles, CA, USA. The research has been funded predominantly by the Alfred Mann Institute at the University of Southern California, Los Angeles, CA, USA; and in part by NIH BRP Grant #R01EB002094. There are no financial relationships that may pose a conflict of interest.

REFERENCES

- ¹Abolhassani, N., R. Patel, and M. Moallem. Needle insertion into soft tissue: a survey. *Med. Eng. Phys.* 29(4): 413–431, 2007. doi:[10.1016/j.medengphy.2006.07.003](https://doi.org/10.1016/j.medengphy.2006.07.003).
- ²Chandrupatla, T. R., and A. D. Belegundu. Introduction to Finite Elements in Engineering (2nd ed.). New Delhi: Prentice-Hall, 1997.
- ³Clements, C. J., M. T. Aguado, and L. Jodar. Technologies to improve immunisation safety [Review]. *Drug Saf.* 24(14):1019–1026, 2001. doi:[10.2165/00002018-200124140-00001](https://doi.org/10.2165/00002018-200124140-00001).
- ⁴Cook, R. D., D. S. Malkus, M. E. Plesha, and R. J. Witt. Concepts and Applications of Finite Element Analysis (4th ed.). New York: John Wiley & Sons, 2002.

- ⁵DiMaio, S. P., and S. E. Salcudean. Needle insertion modeling and simulation. *IEEE Trans. Robot. Autom.* 19(5):864–875, 2003. doi:[10.1109/TRA.2003.817044](https://doi.org/10.1109/TRA.2003.817044).
- ⁶Dupont, A. C., S. D. Bagg, L. L. Baker, J. L. Creasy, C. Romano, D. Romano, F. J. R. Richmond, and G. E. Loeb. First patients with BION implants for therapeutic electrical stimulation. *Neuromodulation* 7:38–47, 2004. doi:[10.1111/j.1525-1403.2004.04005.x](https://doi.org/10.1111/j.1525-1403.2004.04005.x).
- ⁷Dupont, A. C., F. J. R. Richmond, and G. E. Loeb. Prevention of muscle disuse atrophy by low-frequency electrical stimulation in rats. *IEEE Trans. Neural Syst. Rehabil. Eng.* 11(3):218–226, 2003. doi:[10.1109/TNSRE.2003.817674](https://doi.org/10.1109/TNSRE.2003.817674).
- ⁸Kim, H., and J. S. Colton. Fabrication and analysis of plastic hypodermic needles. *J. Med. Eng. Technol.* 29(4): 181–186, 2005. doi:[10.1080/03091900412331289898](https://doi.org/10.1080/03091900412331289898).
- ⁹Lloyd, J. S., and J. B. Miltien. Auto-disable syringes for immunization: issues in technology transfer. *Bull. World Health Organ.* 77(12):1001–1007, 1999.
- ¹⁰Loeb, G. E. and F. J. R. Richmond. BION implants for therapeutic and functional electrical stimulation. In: *Neural Prostheses for Restoration of Sensor and Motor Function*, edited by J. K. Chapin, K. A. Moxon, and G. Gaal. Naples, FL: CRC Press, 2001, pp. 75–99.
- ¹¹Loeb, G. E., F. J. R. Richmond, and L. L. Baker. The BION devices: injectable interfaces with peripheral nerves and muscles. *Neurosurg. Focus* 20(5):E2, 2006.
- ¹²Özkaya, M., and M. Nordin. *Fundamentals of Biomechanics: Equilibrium, Motion, and Deformation* (2nd ed.). New York: Springer, p. 183, 1999.
- ¹³Podder, T. K., J. Sherman, D. P. Clark, E. M. Messing, D. J. Rubens, J. G. Strang, L. Liao, R. A. Brasacchio, Y. Zhang, W. S. Ng, and Y. Yu. Evaluation of robotic needle insertion in conjunction with in vivo manual insertion in the operating room. In: *IEEE International Workshop on Robots and Human Interactive Communication*, 2005, pp. 66–72.
- ¹⁴Simone, C., and A. M. Okamura. Modeling of needle insertion forces for robot-assisted percutaneous therapy. In: *Proc. 2002 Int. IEEE Robotics and Automation Conf.*, 2002, pp. 2085–2091.
- ¹⁵Tan, W., Q. Zou, E. S. Kim, and G. E. Loeb. Sensing human arm posture with implantable sensors. In: *Proc. 26th Int. IEEE Eng. Med. Biol. Conf.*, 2004, pp. 4290–4293.
- ¹⁶Weber, D. J., R. B. Stein, K. M. Chan, G. E. Loeb, F. J. R. Richmond, R. Rolf, K. James, S. L. Chong, A. K. Thompson, and J. Misiaszek. Functional electrical stimulation using microstimulators to correct foot drop: a case study. *Can. J. Physiol. Pharm.* 82:784–792, 2004. doi:[10.1139/y04-078](https://doi.org/10.1139/y04-078).
- ¹⁷World Health Organization. Safety of injections: WHO-UNICEF-UNFPA joint statement on the use of auto-disable syringes in immunizations services. WHO/V&B/99.25, 1999.
- ¹⁸Zou, Q., W. Tan, E. S. Kim, and G. E. Loeb. Single- and triaxis piezoelectric-bimorph accelerometers. *J. Microelectromech. Syst.* 17(1):45–57, 2008. doi:[10.1109/JMEMS.2007.909100](https://doi.org/10.1109/JMEMS.2007.909100).
- ¹⁹Zou, Q., W. Tan, E. S. Kim, J. Singh, and G. E. Loeb. Implantable biaxial piezoresistive accelerometer for sensorimotor control. In: *Proc. 26th Int. IEEE Eng. Med. Biol. Conf.*, 2004, pp. 4279–4282.